




Highly compressible polyimide/graphene aerogel for efficient oil/water separation

Rui-Peng Ren^{1,*} , Zhen Wang¹, Jing Ren¹, and Yong-Kang Lv^{1,*}

¹Key Laboratory of Coal Science and Technology of Ministry of Education and Shanxi Province, Taiyuan University of Technology, Taiyuan 030024, Shanxi, China

Received: 18 October 2018

Accepted: 6 December 2018

Published online:

14 December 2018

© Springer Science+Business Media, LLC, part of Springer Nature 2018

ABSTRACT

Graphene aerogel with three-dimensional (3D) interconnected porous structure and good hydrophobicity has been extensively investigated for sorbent materials for oils and demonstrated to be effective. Herein, a 3D polyimide–graphene aerogel (PI-GA) nanocomposite has been prepared by introducing water-soluble polyimide (PI). Benefiting from the synergetic effect of PI and GA, the PI-GA nanocomposite exhibits ultralow density, excellent compressibility and hydrophobicity. When evaluated as a sorbent material for oils and organic solvent, PI-GA nanocomposite has high absorption capacity and can separate oil from water rapidly and efficiently. Furthermore, the mechanical squeezing process can be used for the recycling of the PI-GA due to its excellent compressibility. The excellent absorption performance and robust mechanical properties make the PI-GA suitable for oil cleanup and chemical leakage.

Introduction

With the increase in the demand of crude oil, more spills and leaks of oil pollutants occur. To solve the environmental and ecological problems arising from the oil spill accidents, it is urgent to develop an effective strategy to realize the separation of oil and water [1–3]. Various strategies such as combustion [4], oil skimmer vessels [5] and sorbents [6, 7] have been proposed to solve the problems. Among these, sorbents are considered as one of the most promising methods [8]. To date, a variety of sorbent materials, such as activated carbon [9], high-oil-absorbing resin [10], fly ash [11], bentonites [12], expanded graphite

[13] and three-dimensional (3D) carbon-based materials have been developed for oil absorption. Compared to other sorbent materials, 3D carbon-based materials show unique advantages, such as low density, high porosity and hydrophobic properties [14, 15], which make them promising candidates for the separation of oil and water.

Graphene aerogel (GA), a representative 3D carbon-based material, has been widely investigated for sorbent material [16–19]. Recently, many endeavors have been made to explore graphene aerogels applying in oil–water separation. Chen et al. [20] developed a simple one-step hydrothermal treatment and freeze-drying approach for the preparation of efficient oil absorbent; its absorption capacity could

Address correspondence to E-mail: renruipeg@tyut.edu.cn; lykang@tyut.edu.cn

maintain at 96% after 20 compression/release cycles. Hong et al. [21] prepared functionalized graphene aerogel by surface modification of self-assembled graphene oxide aerogels. These aerogels had excellent absorption performance for oils and organic solvents (112 g/g) and mechanical strength (supports at least 2600 times its own weight). However, these GAs exhibited brittle mechanical performance when suffering from cyclic compression. The poor cyclic stabilities under compression restrict the widespread applications of GAs for efficient separation spilled oil and water.

Constructing graphene aerogel with excellent mechanical properties and absorption abilities remains a challenge. Polyimide (PI) shows excellent compressible features and thermal stability. Inspired by this, we chose PI to enhance the compressible properties of graphene aerogels. Herein, we fabricate lightweight, hydrophobic and porous PI-GA nanocomposites by introducing PI precursor into graphene oxide (GO) dispersion. Owing to the superior compressible property of PI, the PI-GA nanocomposite show reversible compressibility, high compressibility and mechanical durability. More importantly, the PI-GA exhibits a maximum sorption capacity up to 37.44 times the weight of the pristine PI-GA. In addition, the PI-GA also exhibits the excellent recyclability.

Experimental section

Materials

Natural graphite powder (325 mesh) was provided by Alfa-Aesar Chemical Reagent Co. The H_2SO_4 (98%), NaNO_3 (99%), KMnO_4 , HCl (37%), H_2O_2 (30%) and Sudan Red I were purchased from Tianjin Chemical Reagent Co. Pyromellitic dianhydride (PMDA, 99%), 4,4'-diaminodiphenyl ether (ODA, 98%) and *N,N*-dimethylacetamide (DMAc, 99.5%) were supplied by Shanghai Aladdin Bio-Chem Technology Co., Ltd, and the PMDA was dried in a vacuum oven at 180 °C for 6 h prior to use. Triethylamine (TEA, 99%) was obtained from Tianjin Zhiyuan Chemical Reagent Co., Ltd. All chemicals were used without further purification.

Preparation of GO dispersion

Graphite oxide was prepared from natural graphite according to Hummer's method [22, 23]. In an ice bath, 5 g graphite and 2.5 g NaNO_3 were added to 130 mL H_2SO_4 and stirred vigorously for 2 h. Next, 15 g KMnO_4 was slowly added into the mixture and reacted for 2 h while keeping the temperature below 20 °C. Subsequently, the mixture was heated to 35 °C to react for 0.5 h. After adding 230 mL deionized water dropwise, another 0.5-h reaction was performed at 98 °C. Then, stop heating and add 500 mL deionized water and 5 mL H_2O_2 (30%). Finally, the as-prepared suspension was centrifuged and washed to remove residual salts, GO sheets were collected after drying. The exfoliated GO dispersion (5 mg mL^{-1}) was prepared by ultrasonication of the GO in deionized water for 2 h (Figure S1).

Preparation of water-soluble PI precursor solution

Water-soluble poly(amic acid) (PAA) oligomer, the precursor of PI, was synthesized according to the literature [24]. The procedure was as follows: dispersing 4,4'-ODA in DMAc with a magnetic stirrer. Then, a quantity of PMDA was added into the mixture after 4,4'-ODA was dissolved completely, and the mixture was stirred for 5 h in an ice bath. Note that the 4,4'-ODA/PMDA molar ratio was 99:100. The resulting yellow viscous solution was poured into excess deionized water, and PAA was collected after washing and drying. The water-soluble PI precursor solution with a solid content of 5 wt% was prepared by adding 4 g PAA and 1.92 g TEA into 74.08 g deionized water and stirring the mixture until it became homogeneous and transparent.

Preparation of PI-GA

PI-GA was prepared by two steps: freeze-drying and thermal annealing. Briefly, the water-soluble PI precursor solution was mixed with a certain amount of GO aqueous dispersion (5 mg mL^{-1}), and the volume ratio of the PAA ammonium salt solution to the GO aqueous dispersion was 1:1. Stirring the mixture for 2 h is followed by transferring the mixture to the mold and freeze-drying for 72 h. The resulting monolith was then removed and heated at 400 °C in argon atmosphere for 2 h to obtain PI-GA. Pure PI

aerogel and GA were also prepared by the same procedure.

Materials characterization

The morphology of the fabricated aerogels was observed with a SU 8010 field emission scanning electron microscope (SEM) (Hitachi, Japan) at a voltage of 15 kV. Fourier transform infrared spectroscopy (FT-IR) spectra of the materials and different aerogels were collected in the region of 400–4,000 cm^{-1} using a Nicolet iS 10 FT-IR spectrometer (Thermo Fisher Scientific, USA). X-ray diffraction (XRD) patterns of aerogels were characterized on a MiniFlex II X-ray diffractometer (Rigaku, Japan). ESCALAB 250Xi (Thermo Fisher Scientific, USA) apparatus was used for X-ray photoelectron spectroscopy (XPS) analysis. The contact angle was measured on a JC 2000C Contact Angle Measuring Instrument (POWEREACH, China) at room temperature.

Absorption capacity

The absorption capacities (k_1) of PI-GA to various oils and chemical solvents are calculated by Eq. (1):

$$k_1 = \frac{m_1 - m_0}{m_0} \quad (1)$$

where m_0 (g) and m_1 (g) were weight of aerogel before and after absorption.

Results and discussion

The fabrication process of the PI-GA is illustrated schematically in Fig. 1. First, the PAA-GO aerogel was directly obtained by freeze-drying the aqueous solution of PAA and GO. Then, thermal treatment in argon atmosphere was conducted to reduce the GO to GA and cross-link the PAA into PI simultaneously. Finally, the freestanding and lightweight PI-GA, as displayed in the photograph in Fig. 1b, has dimensions of 24.51 cm^{-3} ($r = 1.7$ cm, $h = 2.7$ cm, in which “ r ” and “ h ” are the base radius and height of PI-GA, respectively) and a weight of 110.5 mg. The low density enables it rest on the top of a dandelion (Fig. 1b).

The morphologies of the pure GA, PI aerogel and PI-GA nanocomposite were characterized by scanning electron microscopy (SEM). As shown in Fig. 2a

and b, the pure GA exhibits an interconnected, porous 3D structure of randomly oriented graphene sheets with continuous macropores ranged from hundreds of nanometers to tens of micrometers. The pore walls are thin, which is constructed by few-layer graphene sheets (Fig. 2b, S2). The SEM observation of PI aerogel shows the same porous structure (Fig. 2c), and the pore wall is composed of PI sheets (Fig. 2d). As for the PI-GA, it possesses the lamellar structures with struts connecting the adjacent layers (Fig. 2e). The 3D skeleton of the PI-GA includes flake-like sheets, which is composed of graphene and PI (Fig. 2f). The macropores are formed between the flakes, where ice is removed during the freeze-drying process. After introducing PI, the pore walls become thicker compared to that of pure GA.

Fourier transform infrared (FT-IR) spectra were obtained to verify the structure variation of the as-prepared samples (Fig. 3a). GO shows three prominent characteristic peaks located at 3357 cm^{-1} , 1732 cm^{-1} and 1622 cm^{-1} , corresponding to the –O–H asymmetric stretching vibrations, C=O stretching vibrations and aromatic C=C stretching vibrations, respectively [25]. Furthermore, two tiny peaks observed at 1406 cm^{-1} and 1058 cm^{-1} can be assigned to –O–H deformation vibrations and C–O stretching vibrations, respectively [26, 27]. These absorption peaks indicate the presence of abundant oxygen-containing groups on the surface of the GO sheets. In the case of GA, the absorption peaks of GO weaken or disappear, suggesting that GO has been reduced into graphene. For PAA and PAA-GO, the characteristic absorption peaks at 1654 cm^{-1} can be attributed to amide C=O stretching vibrations (amide band I), while the peak at 1545 cm^{-1} is assigned to the variable angle vibration of –N–H bonds and the stretching vibrations of C–N bonds (amide band II) (Figure S3). However, for PI sample after imidization, the peaks at 1717 cm^{-1} and 1775 cm^{-1} are belonged to imide C=O symmetric and asymmetric stretching, respectively. Meanwhile, C–N stretching peak is observed at 1378 cm^{-1} . The absence of absorption peaks which belong to amide band I and II suggests the completion of imide cyclization reaction. For the PI-GA nanocomposite, the presence of the similar absorption peaks as PI aerogel indicates that PI has been successfully coated on the GA.

The X-ray diffraction (XRD) patterns of GO present a sharp diffraction peak at $2\theta = 11.13^\circ$, corresponding to the interlayer spacing of 7.95 Å due to the oxygen-

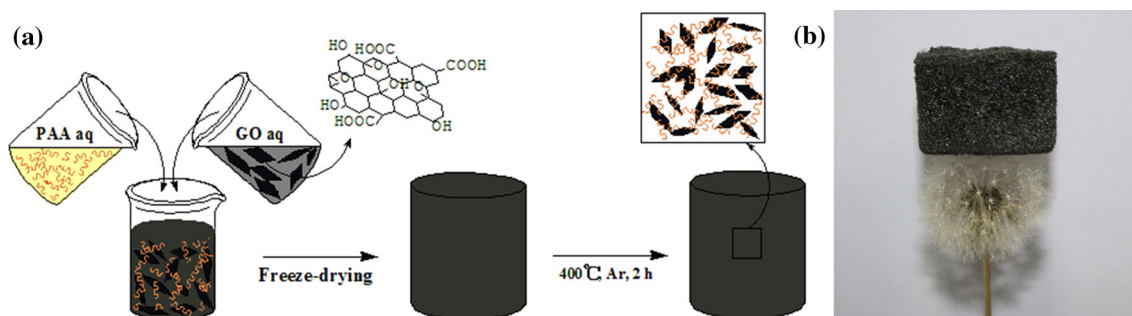


Figure 1 a Schematic diagram for the synthesis of the PI-GA nanocomposite. b PI-GA nanocomposite resting on a dandelion.

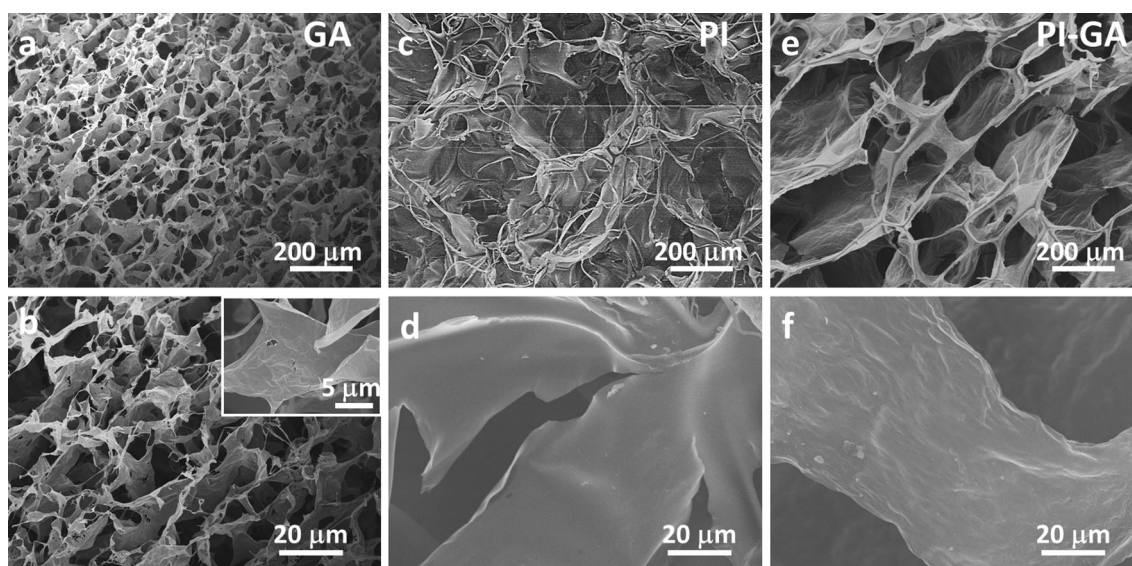


Figure 2 SEM images of the a, b GA, c, d PI aerogel and e, f PI-GA nanocomposite.

containing functional groups on the surface of GO [28]. After thermal reduction, the characteristic peaks of GO disappear, and a new diffraction peak appears at $2\theta = 21.43^\circ$, indicating a high degree of reduction of GO with the interlayer spacing of 0.42 nm. There is no sharp crystal diffraction peak observed in the XRD pattern of PI, indicating that PI is an amorphous polymer [29]. There are two weak peaks at $2\theta = 14.23^\circ$ and 25.64° , manifesting that the molecular chains of PI are still highly ordered [30]. Compared with PI, the two sharp diffraction peaks of PI-GA at $2\theta = 13.54^\circ$ and 16.46° indicate that it has a partially cross-linked structure after the introduction of GA [31].

X-ray photoelectron spectroscopy (XPS) measurement was taken to further study the variation of elemental composition of the as-prepared materials (Fig. 3c, d). The XPS survey spectra of the GO and GA confirm the presence of C and O elements

(Fig. 3c). As shown in Fig. 3d, the intensity of the peak belonging to C located at 284.8 eV increases from GO to GA, while the change in O content (at 532 eV) shows the opposite trend (Table 1). The XPS analysis further confirms the reduction of GO during the thermal treatment process. As for the PI aerogel and PI-GA nanocomposite, a new N 1s peak appears beside the C 1s and O 1s peaks. As shown in Fig. 3d, the high-resolution C 1s spectra of PI aerogel and PI-GA are deconvoluted into four individual component peaks, which can be ascribed to 284.8 eV (C–C/C=C), 285.8 eV (C–N), 286.3 eV (C–O) and 288.6 eV (C=O), respectively [32]. Furthermore, the intensity of the peak corresponding to 284.8 eV (C–C/C=C) of PI-GA increases, while the peak intensities of C–N, C–O and C=O decrease. This means a strong interaction between PI and GA.

Compression experiments were performed, and the compressive stress–strain ($\sigma - \varepsilon$) curves during

Figure 3 **a** FT-IR spectra, **b** XRD patterns, **c** XPS survey spectrum and **d** corresponding high-resolution XPS spectra of C 1s of the GO, GA, PI aerogel and PI-GA nanocomposite.

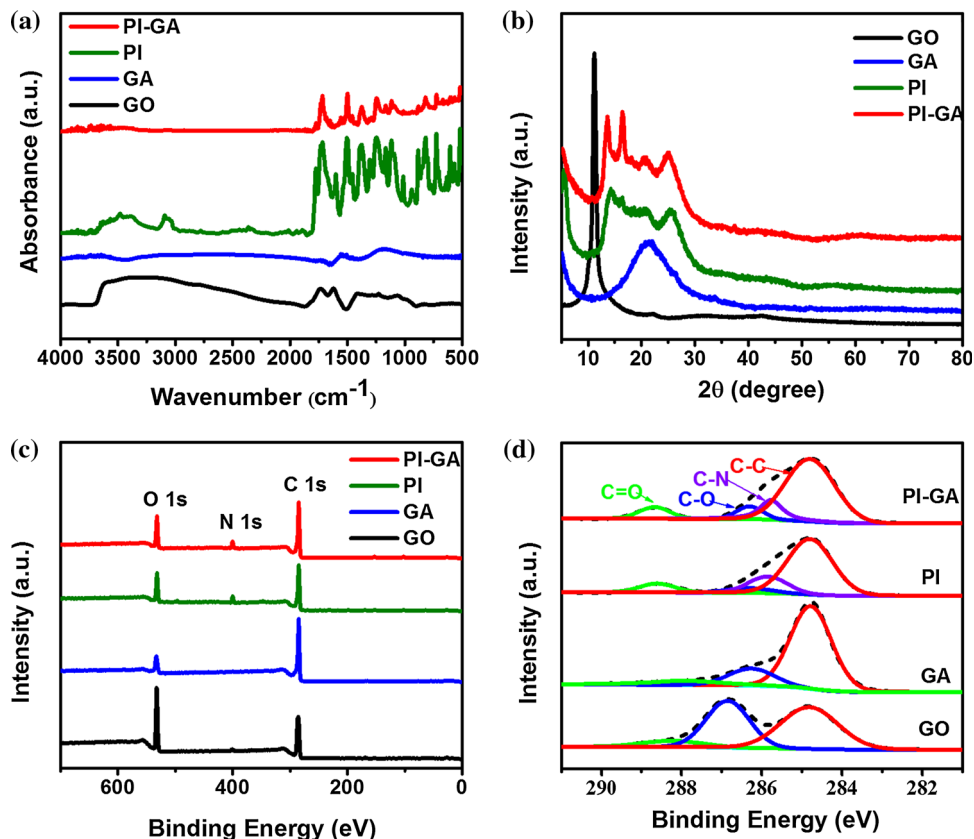


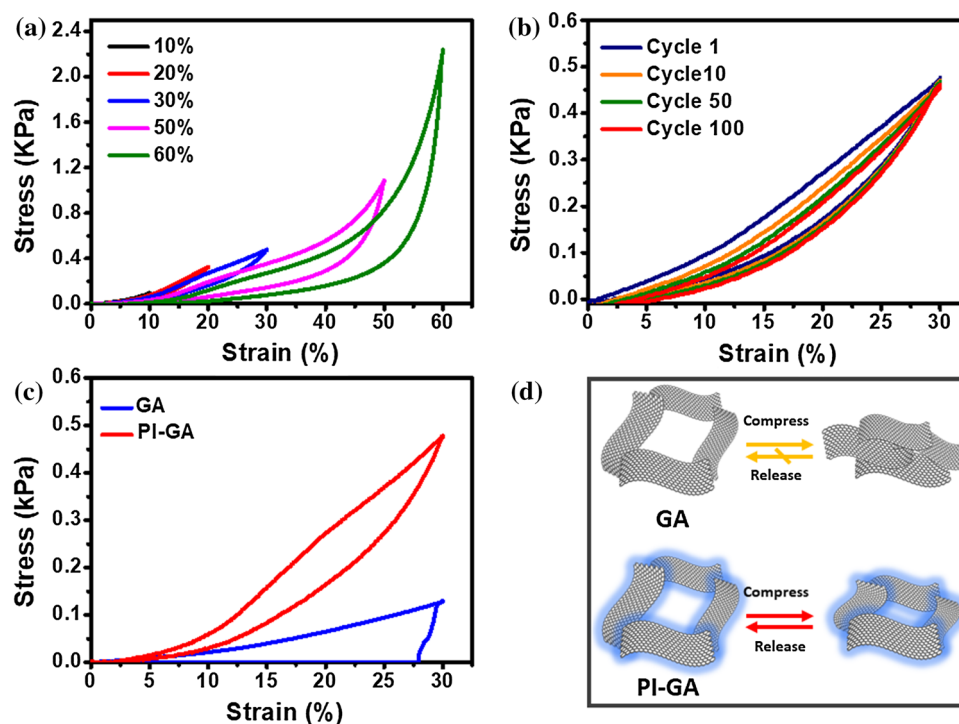
Table 1 Elemental composition of GO, GA, PI and PI-GA

Samples	C atomic concentration (%)	O atomic concentration (%)	N atomic concentration (%)
GO	69.34	30.66	—
GA	87.6	12.4	—
PI aerogel	75.13	18.1	6.77
PI-GA	76.83	17.09	6.08

this process were recorded to study the mechanical properties of the as-prepared materials. The compressive stress–strain curves show three distinct stages during the loading process (Fig. 4a). The compressible region at $\varepsilon < 15\%$ had a linear stress–strain curve, which records the compressible bending of pore walls [33]. The plateau region at $15\% < \varepsilon < 50\%$ has an increased slope, which corresponds to the compressible buckling of the pore walls [34]. And the densification region at $\varepsilon > 50\%$ represents by the rapid increase in stress [35]. Moreover, the stress–strain curve of the 100th cycle almost remains unchanged, and the maximum stress at $\varepsilon = 30\%$ is only 2.3% lower than that of original value (Fig. 4b). These results show the excellent compressibility of the PI-GA nanocomposite. To further demonstrate the structural advantages of PI-GA

nanocomposite, GA is used as control sample to compare their mechanical properties. As shown in Fig. 4c, both GA and PI-GA can be compressed to 30% strain. Once the external pressure is removed, the PI-GA can completely recover, while the GA can recover only partially (5% strain). Tangent modulus is defined as the slope of a line tangent to the stress–strain curve at a point of interest, which is equal to the Young’s modulus at zero strain. The higher Young’s modulus of PI-GA (0.30 kPa) than that of GA (0.19 kPa) can be attributed to the strong inter-atomic interactions. In addition, the yielding behavior is not observed for the PI-GA and GA. Although there is no yielding behavior, the Young’s modulus of PI-GA decreases during the subsequent cycling tests (Figure S4), which is due to the viscoelasticity of the polymer [36]. The brittle feature of GA can be

Figure 4 **a** Stress–strain curves of PI-GA at different maximum strain of 10%, 20%, 30%, 50% and 60%, respectively. **b** Stress–strain curves of PI-GA at the maximum strain of 30% for 100 cycles. **c** Comparison of the stress–strain curves of GA and PI-GA. **d** Compressive schematic of GA and PI-GA nanocomposite.



ascribed to that the graphene sheets are jointed together by the relatively weak van der Waals forces, and it can collapse easily during compression. As for the PI-GA, the strong interactions between PI and GA enable its excellent compressibility (Fig. 4d).

Water contact angle (CA) measurement was taken to investigate the wettability of the PI-GA, and it exhibits surface hydrophobicity with a water CA of 136° (Fig. 5a). Therefore, the PI-GA possesses high hydrophobicity, which is beneficial for selective uptake of oils and organic solvents [37]. Owing to the low density, high porosity, excellent compressibility and surface hydrophobicity, the PI-GA is considered as a promising material for the sorption of oils and organic solvents [38]. The excellent sorption capability of PI-GA is demonstrated in Fig. 5b. When PI-GA contacts with a drop of oil on water surface, the oil is completely absorbed by PI-GA in a short time and PI-GA still remains floating on the water surface, which implies its potential application in the removal of oil spillage and the ease for recycling. To further evaluate the absorption capacity quantitatively, the weight gain, wt%, is defined as the weight of absorbed substance per unit weight of the PI-GA. We investigated the absorption capacity of the PI-GA for several kinds of oils and organic solvents including motor oil, ethanol, acetone, dimethylcarbinol, methyl methacrylate (MMA), ethylene glycol and n-hexyl

alcohol. The absorption capacity of PI-GA is calculated by Eq. (1). As displayed in Fig. 5c, PI-GA shows remarkable absorption abilities toward a wide range of oils and organic solvents. In general, the absorption capacity ranges from 22.94 to 37.44 g/g, depending on the surface tension and density of the liquids tested. Therefore, these results suggest that PI-GA nanocomposite is an ideal absorbent for removal of oil spill and organic solvents pollution in water.

For practical applications, the recyclability of the absorbent was great key parameter for the removal of oil spills. Furthermore, compared to the absorption–combustion method [39, 40], the absorption–squeezing method made the reutilization of absorbed oils and organic solvents. The excellent compressibility of PI-GA facilitates the squeezing process and the reutilization of absorbed oils and organic solvents. Therefore, the cyclic absorption–squeezing behavior of PI-GA was investigated using motor oil as model adsorbate, as shown in Fig. 5d. As predicted, Fig. 5e shows that PI-GA not only exhibits excellent absorption capacity, but also possesses highly recyclability of absorbed oils during 10 cycles. During the repeated absorption–squeezing cycles, the oil absorption capacity of PI-GA still remains stable (≥ 34 g/g) [41]. Therefore, PI-GA

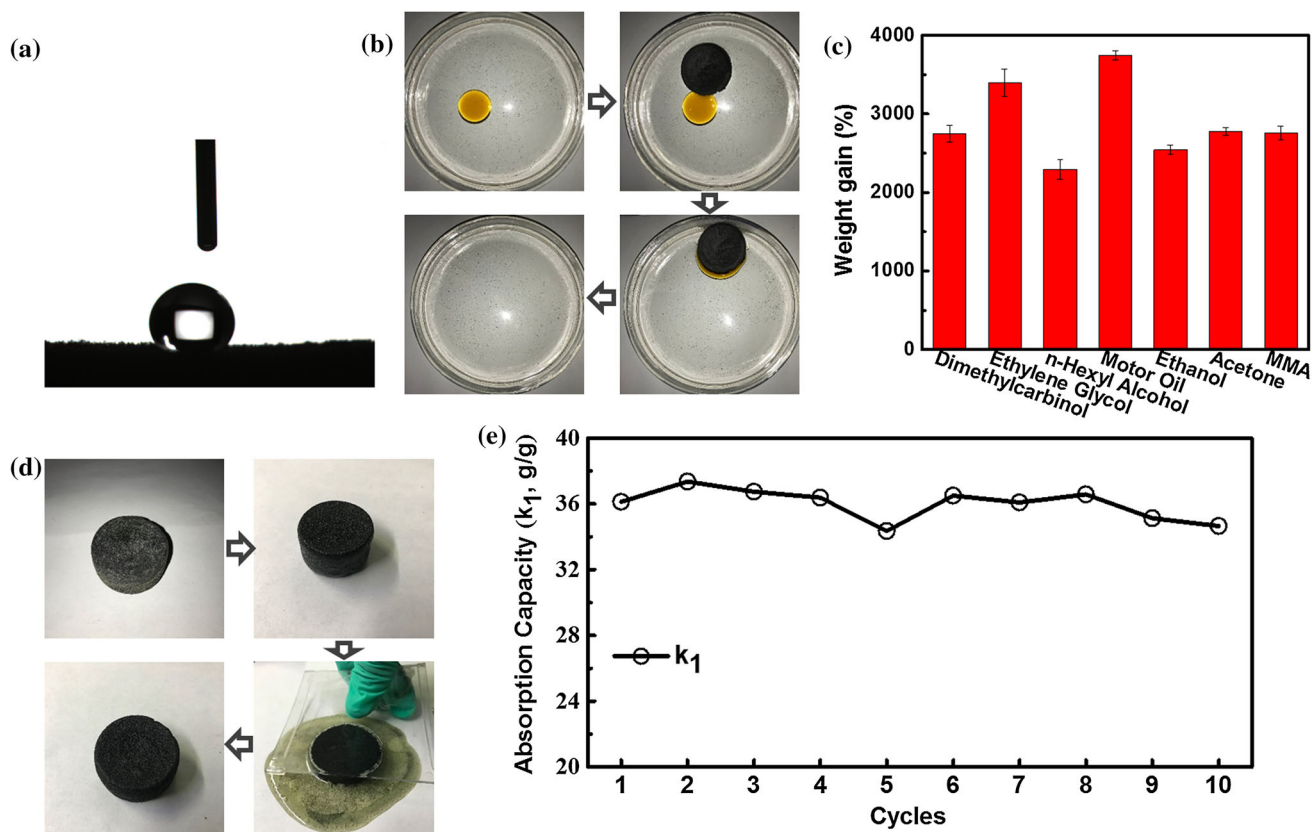


Figure 5 a Optical image of a water droplet on the surface of the PI-GA. b Photographs of the removal process of motor oil (dyed with Sudan Red I) from the surface of water with PI-GA. c Absorption capacity of PI-GA for various oils and chemical

nanocomposite shows great potential applications in recyclable removal of oils and organic solvents.

Conclusion

In summary, we have demonstrated the fabrication of compressible PI-GA nanocomposite by introducing water-soluble PI precursor into GO aqueous dispersion. The PI-GA nanocomposite not only can take full advantages of each component but also can bring synergetic effects, which exhibits hydrophobicity and excellent compressibility. When used as an absorbent material, it shows high absorption capacity (22.94–37.44 g/g). Due to its excellent compressibility, the mechanical squeezing process can be used for the recycling of the PI-GA. Therefore, the PI-GA nanocomposite shows great potential applications in economic, efficient and safe absorbent for environmental and ocean protection.

solvents. d Photographs showing the process of recycling PI-GA nanocomposite via mechanical squeezing. e Recycling performance of PI-GA for absorption of motor oil by absorption/mechanical squeeze processes.

Acknowledgements

This work was supported by the National Natural Science Foundation of China (21406154, 21776196, 51778397).

Electronic supplementary material: The online version of this article (<https://doi.org/10.1007/s10853-018-03238-1>) contains supplementary material, which is available to authorized users.

References

- [1] Huang H, Liu M, Li Y, Yu Y, Yin X, Wu J, Chen S, Xu J, Wang L, Wang H (2018) Polyphenylene sulfide microfiber membrane with superhydrophobicity and superoleophilicity for oil/water separation. *J Mater Sci* 53:13243–13252. <https://doi.org/10.1007/s10853-018-2546-3>

- [2] Wang E, Wang H, Liu Z, Yuan R, Zhu Y (2015) One-step fabrication of a nickel foam-based superhydrophobic and superoleophilic box for continuous oil–water separation. *J Mater Sci* 50:4707–4716. <https://doi.org/10.1007/s10853-015-9021-1>
- [3] Wang H, Yang J, Liu X, Tao Z, Wang Z, Yue R (2019) A robust 3D superhydrophobic sponge for in situ continuous oil removing. *J Mater Sci* 54:1255–1266. <https://doi.org/10.1007/s10853-018-2938-4>
- [4] Bi H, Yin Z, Cao X, Xie X, Tan C, Huang X, Chen B, Chen F, Yang Q, Bu X, Lu X, Sun L, Zhang H (2013) Carbon fiber aerogel made from raw cotton: a novel, efficient and recyclable sorbent for oils and organic solvents. *Adv Mater* 25:5916–5921
- [5] Yan C, Ji Z, Ma S, Wang X, Zhou F (2016) 3D printing as feasible platform for on-site building oil-skimmer for oil collection from spills. *Adv Mater Interfaces* 3:1600015
- [6] Ge J, Zhao H, Zhu H, Huang J, Shi L, Yu S (2016) Advanced sorbents for oil-spill cleanup: recent advances and future perspectives. *Adv Mater* 28:10459–10490
- [7] Yuan J, Gao R, Wang Y, Cao W, Yun Y, Dong B, Dou J (2018) A novel hydrophobic adsorbent of electrospun SiO₂@MUF/PAN nanofibrous membrane and its adsorption behaviour for oil and organic solvents. *J Mater Sci* 53:16357–16370. <https://doi.org/10.1021/acs.jpcc.5b00662>
- [8] Shiu RF, Lee CL, Hsieh PY, Chen CS, Kang YY, Chin WC, Tai NH (2018) Superhydrophobic graphene-based sponge as a novel sorbent for crude oil removal under various environmental conditions. *Chemosphere* 207:110–117
- [9] Rasouli Y, Abbasi M, Hashemifard SA (2017) Oily wastewater treatment by adsorption-membrane filtration hybrid process using powdered activated carbon, natural zeolite powder and low cost ceramic membranes. *Water Sci Technol* 76:895–908
- [10] Sun J, Xu Y, Chen H, Tan Z, Fan L (2014) Synthesis and properties of high oil-absorbing resins with long chain by high internal phase emulsions as template. *Sep Sci Technol* 49:2518–2524
- [11] Wang W, Ye Z, Li F (2016) Removal of oil from simulated oilfield wastewater using modified coal fly ashes. *Desalin Water Treat* 57:9644–9650
- [12] Kumar S, Mandal A, Guria C (2016) Synthesis, characterization and performance studies of polysulfone and polysulfone/polymer-grafted bentonite based ultrafiltration membranes for the efficient separation of oil field oily wastewater. *Process Saf Environ* 102:214–228
- [13] Ding XH, Wang R, Zhang X et al (2014) A new magnetic expanded graphite for removal of oil leakage. *Mar Pollut Bull* 81:185–190
- [14] Han Q, Yang L, Liang Q, Ding M (2017) Three-dimensional hierarchical porous graphene aerogel for efficient adsorption and preconcentration of chemical warfare agents. *Carbon* 122:556–563
- [15] Chen B, Ma Q, Tan C, Lim T, Huang L, Zhang H (2015) Carbon-based sorbents with three-dimensional architectures for water remediation. *Small* 11:3319–3336
- [16] Li Y, Li L, Chen T, Duan T, Yao W, Zheng K, Dai L, Zhu W (2018) Bioassembly of fungal hypha/graphene oxide aerogel as high performance adsorbents for U(VI) removal. *Chem Eng J* 347:407–414
- [17] Hu H, Zhao Z, Wan W, Gogotsi Y, Qiu J (2013) Ultralight and highly compressible graphene aerogels. *Adv Mater* 25:2219–2223
- [18] Zhang X, Liu P, Duan Y, Jiang M, Zhang J (2017) Graphene/cellulose nanocrystals hybrid aerogel with tunable mechanical strength and hydrophilicity fabricated by ambient pressure drying technique. *RSC Adv* 7:16467–16473
- [19] Lu K, Yuan L, Xin X, Xu Y (2018) Hybridization of graphene oxide with commercial graphene for constructing 3D metal-free aerogel with enhanced photocatalysis. *Appl Catal B Environ* 226:16–22
- [20] Chen C, Li F, Zhang Y, Wang B, Fan Y, Wang X, Sun R (2018) Compressive, ultralight and fire-resistant lignin-modified graphene aerogels as recyclable absorbents for oil and organic solvents. *Chem Eng J* 350:173–180
- [21] Hong JY, Sohn EH, Park S, Park HS (2015) Highly-efficient and recyclable oil absorbing performance of functionalized graphene aerogel. *Chem Eng J* 269:229–235
- [22] Marcano DC, Kosynkin DV, Berlin JM, Sinitskii A, Sun Z, Slesarev A, Alemany LB, Lu W, Tour JM (2010) Improved synthesis of graphene oxide. *ACS Nano* 4:4806–4814
- [23] Shi Y, Li C, He D, Shen L, Bao N (2017) Preparation of graphene oxide–cellulose acetate nanocomposite membrane for high-flux desalination. *J Mater Sci* 52:13296–13306. <https://doi.org/10.1007/s10853-017-1403-0>
- [24] Wu W, Wang K, Zhan M (2012) Preparation and performance of polyimide-reinforced clay aerogel composites. *Ind Eng Chem Res* 51:12821–12826
- [25] Ramakrishnan S, Dhakshnamoorthy M, Jelmy EJ, Vasanthakumari R, Kothurkar NK (2014) Synthesis and characterization of graphene oxide-polyimide nanofiber composites. *RSC Adv* 4:9743–9749
- [26] Zhang Y, Huang Y, Yang G, Bu F, Li K, Shakir I, Xu Y (2017) Dispersion-assembly approach to synthesize three-dimensional graphene/polymer composite aerogel as a powerful organic cathode for rechargeable Li and Na batteries. *ACS Appl Mater Inter* 9:15549–15556

- [27] Yoonessi M, Gaier JR (2010) Highly conductive multi-functional graphene polycarbonate nanocomposites. *ACS Nano* 4:7211–7220
- [28] Li C, Jiang D, Liang H, Huo B, Liu C, Yang W, Liu J (2018) Superelastic and arbitrary-shaped graphene aerogels with sacrificial skeleton of melamine foam for varied applications. *Adv Funct Mater* 28:1704674
- [29] Zhang Y, Fan W, Huang Y, Zhang C, Liu T (2015) Graphene/carbon aerogels derived from graphene cross-linked polyimide as electrode materials for supercapacitors. *RSC Adv* 5:1301–1308
- [30] Upadhyay R, Steudel S, Hung MP, Mandal AK, Catthoor F, Nag M (2018) Self-aligned amorphous indium-tin-zinc-oxide thin film transistors on polyimide foil. *ECS J Solid State Sci* 7:185–191
- [31] Kwon K, Chang JH (2015) Comparison of the properties of polyimide nanocomposites containing three different nanofillers: organoclay, functionalized graphene, and organoclay/functionalized graphene complex. *J Compos Mater* 49:3031–3044
- [32] Qin Y, Peng Q, Ding Y, Lin Z, Wang C, Li Y, Xu F, Li J, Yuan Y, He X, Li Y (2015) Lightweight, superelastic, and mechanically flexible graphene/polyimide nanocomposite foam for strain sensor application. *ACS Nano* 9:8933–8941
- [33] Jiang D, Li C, Yang W, Zhang J, Liu J (2017) Fabrication of an arbitrary-shaped and nitrogen-doped graphene aerogel for highly compressible all solid-state supercapacitors. *J Mater Chem A* 5:18684–18690
- [34] Xiang Y, Liu L, Li T, Dang Z (2016) Compressible, amphiphilic graphene-based aerogel using a molecular glue to link graphene sheets and coated-polymer layers. *Mater Des* 110:839–848
- [35] Lv P, Tang X, Wei W (2017) Graphene/MnO₂ aerogel with both high compression-tolerance ability and high capacitance, for compressible all-solid-state supercapacitors. *RSC Adv* 7:47116–47124
- [36] Hong JY, Bak BM, Wie JJ, Kong J, Park HS (2015) Reversibly compressible, highly elastic, and durable graphene aerogels for energy storage devices under limiting conditions. *Adv Funct Mater* 25:1053–1062
- [37] He J, Zhao H, Li X, Su D, Zhang F, Ji H, Liu R (2018) Superelastic and superhydrophobic bacterial cellulose/silica aerogels with hierarchical cellular structure for oil absorption and recovery. *J Hazard Mater* 346:199–207
- [38] Tao G, Zhang L, Hua ZL, Chen Y, Guo L, Zhang J, Shu Z, Gao J, Chen H, Wu W, Liu Z, Shi J (2014) Highly efficient adsorbents based on hierarchically macro/mesoporous carbon monoliths with strong hydrophobicity. *Carbon* 66:547–559
- [39] Ren RP, Li W, Lv YK (2017) A robust, superhydrophobic graphene aerogel as a recyclable sorbent for oils and organic solvents at various temperatures. *J Colloid Interf Sci* 500:63–68
- [40] Wang C, Yang S, Ma Q, Jia X, Ma P (2017) Preparation of carbon nanotubes/graphene hybrid aerogel and its application for the adsorption of organic compounds. *Carbon* 118:765–771
- [41] Mi HY, Jing X, Politowicz AL, Chen E, Huang HX, Turng LS (2018) Highly compressible ultra-light anisotropic cellulose/graphene aerogel fabricated by bidirectional freeze drying for selective oil absorption. *Carbon* 132:199–209